A&A 562, A46 (2014)
DOI: 10.1051/0004-6361/201321988


Astronomy & Astrophysics

# Near-infrared spectroscopy of Miranda

F. Gourgeot[1,2], C. Dumas[2], F. Merlin[1,3], P. Vernazza[4], and A. Alvarez-Candal[2,5,6]

[1] Observatoire de Paris-Meudon / LESIA, 92190 Meudon, France
e-mail: florian.gourgeot@obspm.fr
[2] European Southern Observatory, Alonso de Córdova 3107, 1900 Casilla Vitacura, Santiago, Chile
[3] Université Denis Diderot, Paris VII, 75013 Paris, France
[4] Observatoire Astronomique Marseille-Provence, 13013 Marseille, France
[5] Instituto de Astrofísica de Andalucía – CSIC, Glorieta de la Astronomía S/N, 18008 Granada, Spain
[6] Observatório Nacional, COAA, Rua General José Cristino 77, 20921-400 Rio de Janeiro, Brazil

Received 29 May 2013 / Accepted 16 October 2013

**ABSTRACT**

*Aims.* We present new near-infrared spectra of the leading and trailing hemispheres of Uranus's icy satellite Miranda. This body is probably the most remarkable of all the satellites of Uranus, because it displays series of surface features such as faults, craters, and large-scale upwelling, a remnant of a geologically very active past.
*Methods.* The observations were obtained with PHARO at Palomar and SpeX at the IRTF Observatory. We performed spectral modelings to further constrain the nature and the chemical and physical states of the compounds possibly present on the surface of Miranda.
*Results.* Water ice signatures are clearly visible in the *H* and *K* bands, and it appears to be found in its crystalline state over most of the satellite's surface. Unlike what has been found for Uranus's outer moons, we did not find any significative differences in the abundances of ices covering the leading and trailing hemispheres of Miranda. The signature of carbon dioxide cannot be seen in our spectra, which could still account for the presence of ammonia hydrate, though in small amounts.

**Key words.** planets and satellites: surfaces – infrared: planetary systems

## 1. Introduction

Among the various populations of small outer solar system bodies, planetary satellites play an important role in our understanding of planet formation. Recent models (Crida & Charnoz 2012) show that most of the regular satellites formed within planetary tidal disks while the planet's ring particles migrated beyond the Roche limit. In this context, a comparative study between Miranda and the outer moons of Uranus could provide some precious information about the formation and evolution of planetary satellites as a whole. Water, which is the primary "volatile" present in its solid state beyond the Jupiter's snow line, is also the main compound found on the Uranian satellites (Brown & Cruikshank 1983). The largest of them, Ariel, Umbriel, Titania, and Oberon, show possible signs of resurfacing processes, including for Miranda, the innermost and smallest of the regular satellites of Uranus, whose Voyager 2 returned images of a highly perturbed geology with many surface cracks and faults possibly caused by the large-scale motion of some distinct regions on its surface. Such activity is believed to be the result of tidal forces with Uranus and Umbriel, which heated the interior ice and generated upwelling of material (Tittemore & Wisdom 1990). Miranda may have also once been in a 5:3 resonance with Ariel, which could have contributed to its internal heating, although not as efficiently (Tittemore & Wisdom 1990).

The first near-IR spectrum of Miranda was obtained during the Voyager 2 flyby, and it revealed the strong 2.0 $\mu$m feature unambiguously attributed to water ice (Brown & Clark 1984). The geometric albedo $\rho_v$ was measured to slightly vary across the surface, from 0.30 (old and heavily cratered terrains) to 0.37 (more recent, less cratered), with an average of $\rho_v \sim 0.33$ (Buratti & Mosher 1991). As for Saturn's satellite Enceladus, cryovolcanism may play a major role in the resurfacing of Miranda (Karkoschka 1997; Trilling & Brown 2000). Spectral modeling applied on more recent UKIRT data (Bauer et al. 2002) reports the presence of crystalline water ($H_2O$) and ammonia-hydrate ($NH_3.H_2O$) ices, along with some unidentified darker material.

In this paper we present new spectra of Miranda obtained from two different instruments, PHARO (at the 5 m Hale telescope, Palomar Observatory) and SpeX (IRTF, Mauna Kea Observatory). First, we describe the observations and data reduction methods for each instrument. Then we discuss the results of applying bi-hemispherical reflectance models (Hapke 1993) to our data set to analyze the nature and physical state of the chemical compounds possibly present on the surface of Miranda.

**Table 1.** Spectroscopic instrumental configurations used at Palomar and IRTF observatories.

| Instrument | PHARO | SpeX |
|---|---|---|
| Observatory | Palomar | Mauna Kea |
| Telescope | 5.1 m-Hale | 3.0 m-IRTF |
| Spectral range | 1.5–2.5 $\mu$m | 0.8–2.4 $\mu$m |
| Spectral resolution | ~1500 | ~2000 |
| Spatial scale | 0.040″/pix | 0.12″/pix |
| Slit width | 0.52″ | 0.3″ |

## 2. Spectroscopic observations

### 2.1. 5 m Palomar

The observations were performed during two consecutive nights on 2000 August 12 (9h30 UT: *H*-band) and 2000 August 13

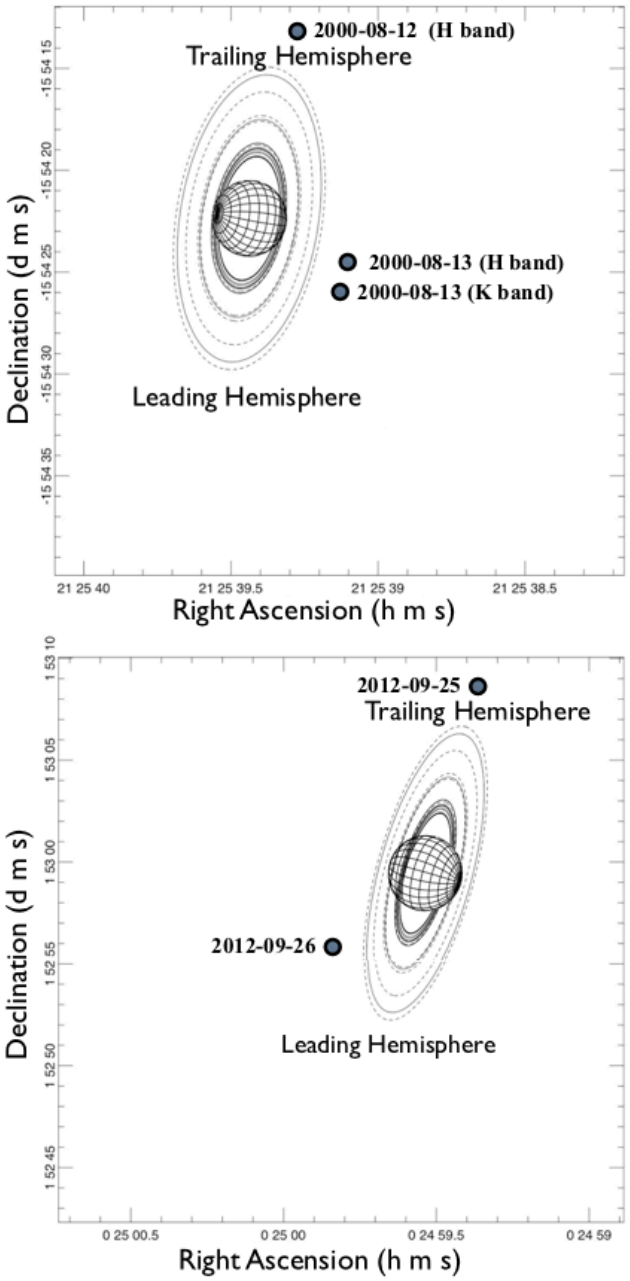


**Fig. 1.** Orbital positions of Miranda for our four observation epochs. On *the top*, data from PHARO in 2000 before the Uranus equinox (2007), and on *the bottom*, observations performed with the SpeX instrument in 2012 after the Uranus equinox. Uranus' drawing source: http://pds-rings.seti.org/

(09h30 UT: $K$ band, and 10h45 UT: $H$-band) using the near-infrared camera PHARO (Palomar High Angular Resolution Observer). This instrument is mounted at the Cassegrain focus of the 5 m Hale telescope and is equipped with a $1024 \times 1024$ pixels HgCdTe HAWAII detector covering a spectral range between 1 and 2.5 $\mu$m and the PALAO adaptive optics system built at NASA-JPL. We used the $H$ and $K$ gratings and a slit width of 0.52″ to image the spectra onto the detector (40 mas/pix) with a spectral resolution of ∼1500. The slit was oriented in a perpendicular direction to the line joining the planet and the satellite. The spectral range is [1.49–1.78] $\mu$m for the $H$-band, and [2.03–2.37] $\mu$m for the $K$-band, with dispersions of 2.84 Å pixel$^{-1}$ and 3.32 Å pixel$^{-1}$, respectively. Figure 1 shows the distinct orbital positions of Miranda for the observation dates. The observation logs for all epochs are reported in Table 2.

### 2.2. IRTF

We observed Miranda on 2012 September 25 and 26 with the SpeX instrument equipping the Infra-Red Telescope Facility (IRTF) at Mauna Kea Observatory. The observations were performed remotely from the ESO headquarters in Garching, Germany. We used the short-wavelength (0.8–2.5 microns) cross-dispersed mode with a 0.8″ slit width (resolving power of ∼2000) and was placed perpendicular to the line joining Uranus and Miranda like the previous observations. The meteo conditions were good at both epochs, with a near-infrared seeing <0.6″ for an airmass lower than 1.5. The MORIS CCD camera, fed by a dichroic located inside SpeX, was used as a facility guider at visible wavelengths.

Although the 2000 Palomar and 2012 IRTF observations were obtained at nearly the same longitudes of Miranda, the sub-Earth latitudes differed between the two epochs. Indeed, owing to Uranus' orbital period of 84 years and to its high obliquity (98°, Seidelmann et al. 2007), the observations of 2000 and 2012 were obtained apart from the equinox (2007 December 7). As a result, Miranda showed its southern hemisphere in 2000 (Palomar observations), while its northern hemisphere was viewed in 2012 (IRTF). For comparison, the Voyager 2 flyby happened in 1986, close to solstice. Since the satellite's rotational period (1.413 days ≈ 33.92 h) is synchronized with its revolution around Uranus, we could still cover a large part of Miranda's surface with observations scheduled only over two consecutive days.

## 3. Data reduction

### 3.1. PHARO

We developed our own IDL routines to reduced the PHARO data. Dark frames were used to make the bad pixel map, while the wavelength calibration was done using the atmospheric emission lines present in our data and comparing their position with tables of OH sky emission lines from the Cool Grating Spectrometer 4 (CGS4) catalog. The precision obtained is estimated to be 1.1 nm, corresponding to an error of five pixels. We followed the procedure described by Metchev & Hillenbrand (2004) to flat-field our spectra. Indeed, spectroscopic flat-field frames were not obtained for each setup. Instead the frames for the science and telluric-standards were divided by their corresponding broad-band imaging flat field. For each set of science spectra, calibration spectra of a telluric standard star were obtained at the exact same position of the detector. Our data set for atmospheric absorptions and solar color will be corrected by dividing the science spectra by the telluric-standard spectra obtained at the same airmass.

Science (Miranda) and calibration (telluric standard) targets were observed at two well-separated positions (e.g., named A & B) along the slit. Both A & B frames were then subtracted from each other to remove the background and correct our data from the sky emission contribution. Any residual flux remaining after the sky emission subtraction was removed by fitting its contribution on both sides of the target spectra. The same technique was applied to remove straylight residual from nearby Uranus in our $H$-band spectra of 2000 August 13.

The extraction of the spectra was itself performed using Image Reduction and Analysis Facility (IRAF) tools. The

**Table 2.** Spectroscopic observations of Miranda (top) and the observed solar analogs (bottom).

| Instrum. | Sub-Earth long.; lat. of Miranda (°) | *TI** (%) | Date [yyyy/mm/dd] | UT time | Band | Exposure time [s] | Number of frames | Airmass | NIR seeing (″) |
|---|---|---|---|---|---|---|---|---|---|
| PHARO | 254.8; –34,4 | 26 | 2000/08/12 | 09h30 | *H* | 300 | 9 | 1.6–1.9 | 0.4 |
| PHARO | 150.3; –34.5 | 15 | 2000/08/13 | 09h20 | *K* | 300 | 15 | 1.6–2.2 | 0.4 |
| PHARO | 162.7; –34.5 | 16 | 2000/08/13 | 10h45 | *H* | 300 | 6 | 2.3–2.8 | 0.4 |
| SpeX | 256.1; +21.4 | 72 | 2012/09/25 | 09h30 | *IJHK* | 120 | 46 | 1.1–1.5 | <0.6 |
| SpeX | 152.6; +21.4 | 60 | 2012/09/26 | 09h40 | *IJHK* | 120 | 32 | 1.1–1.4 | <0.6 |
| HD198802 | (G1V) $Mag_H$ = 4.9 | | 2000/08/12 | 10h45 | *H* | 4 | 20 | 2.50–2.60 | n/a |
| HD220957 | (G7) $Mag_H$ = 4.4 | | 2000/08/13 | 10h20 | *H* | 10 | 8 | 1.75–2.0 | n/a |
| BS06917 | (A2) $Mag_H$ = 5.6 | | 2000/08/13 | 11h40 | *K* | 10 | 24 | ~1.70 | n/a |
| BD-004557 | (F8) $Mag_H$ = 8.3 | | 2012/09/25 | 10h10 | *IJHK* | 30 | 6 | ~1.2 | <0.6 |
| BD-004557 | (F8) $Mag_H$ = 8.3 | | 2012/09/26 | 10h50 | *IJHK* | 30 | 6 | ~1.1 | <0.6 |

**Notes.** Magnitudes are in *H*-band (from SIMBAD: http://simweb.u-strasbg.fr/simbad). (*) *Terra Incognita*: percentage of the visible disk corresponding to regions not imaged by Voyager 2 (at a given epoch).

aperture width for the spectrum was set to the FWHM of the spectra. Pixels within this aperture were summed along the detector columns (which are nearly perpendicular to the dispersion axis), and the center of the dispersed spectra was fitted by a Legendre polynomial function of order 5.

We then combined the individual science and solar analog spectra by airmass bin (see Table 2) prior to divide the spectra of Miranda by that of the solar analog. These spectra, corrected from solar and telluric signatures, were then normalized and combined to produce the final spectrum. Error bars across the spectral range were derived from the dispersion of the individual spectra. Residual noise was removed by applying a median filter and replacing the bad pixels by their corresponding median value. We degraded the spectral resolution $\lambda/\Delta\lambda$ from 1500 to about 750 by convolving the spectrum with a Gaussian filter of $FWHM \sim 1.73$ nm.

### 3.2. SpeX

The IRTF data were reduced using tools provided by the instrument pipeline (Xspextool Version 3.4, Cushing et al. 2004; Rayner et al. 2003) and custom-made IDL routines. The master flat and arc frames were obtained by median-combining all the respective calibration images. For each spectral mode, wavelength calibration was performed by cross-correlating the arc files with a reference arc spectrum with known wavelength solution. The precision of the wavelength calibration is estimated to be better than 1.0 nm. The various spectral orders were extracted using the instrument pipeline. All remaining bad pixels were removed by applying a median filter, and the spectra were combined as described for the PHARO data. The same procedure was employed for the Miranda and solar analog spectra (see Table 2). The spectral resolution of the IRTF data is estimated to be close to 2000.

As for the *H*-band Palomar data of 2000 August 13, the proximity of Uranus from the satellite contaminated the IRTF spectra of Miranda for the date 2012 september 26, when the distance between the two bodies was minimal. Specifically the halo of stray light was clearly visible over several spectral regions: [0.90–0.95] $\mu$m, [1.15–1.20] $\mu$m, [1.25–1.30] $\mu$m, [1.52–1.57] $\mu$m, and [1.58–1.64] $\mu$m. For each of these spectral regions, the contamination was modeled using the signal present on both sides of Miranda's spectrum, and then subtracted from the individual frames.

## 4. Results

### 4.1. Identification of spectral features

Figures 2 and 3 show the full set of reduced spectra of Miranda obtained at Palomar and IRTF. The spectra have been normalized to unity at 1.7 $\mu$m. The images in the left-hand panels of these figures show the location of the sub-Earth points on Miranda's surface for all observation epochs and associated spectral wavebands. The solid gray area represents the portions of Miranda's surface not imaged by Voyager 2. The apparent planetographic longitude and latitude (IAU2006 model) of the sub-Earth points is also given. The spectra on the right-hand side panels of the figures are shown with one-sigma error-bars and are offset from each other by two units along the vertical axis for clarity.

As expected from Miranda's low density ($1.20 \pm 0.15$ g/cm$^3$, Jacobson et al. 1992), the satellite is mainly composed of icy material, with water ice the main constituent. The large 1.5 and 2.0 $\mu$m water ice absorptions are clearly visible in our *H*- and *K*-band data. The weaker feature near 1.65 $\mu$m, which was first detected on Miranda by Bauer et al. (2002), is also visible. This feature informs us that part of the water ice present on Miranda is found in its crystalline state (Schmitt et al. 1998; Grundy & Schmitt 1998), which means that the ice temperature reached a high enough level in the history of Miranda to allow the water ice molecules to organize onto a crystalline lattice. The ammonia hydrate absorption also reported by Bauer et al. (2002) in the 2.22 $\mu$m region is not readily seen in our data and is discussed later in Sect. 4.4. The peak feature seen at 2.0 $\mu$m in the Spex data is a residual from an incomplete correction of the telluric absorptions.

### 4.2. Absence of $CO_2$

We searched for the presence of $CO_2$ ice in our spectra. Figure 4 shows a comparison between Miranda and the four largest moons of Uranus (Grundy et al. 2006), with the positions of the $CO_2$ bands clearly marked. An additional $CO_2$ ice model (also from Grundy et al. 2006) is included for comparison. The spectra of Miranda do not appear to display any signature of $CO_2$ ice on the surface. This result is quite interesting since $CO_2$ ice is increasingly present on the spectra of the trailing hemispheres of Titania, Umbriel, and Ariel, suggesting an external source of contamination linked to the decreasing planetocentric distance of the satellites (Grundy et al. 2006). The relatively small size

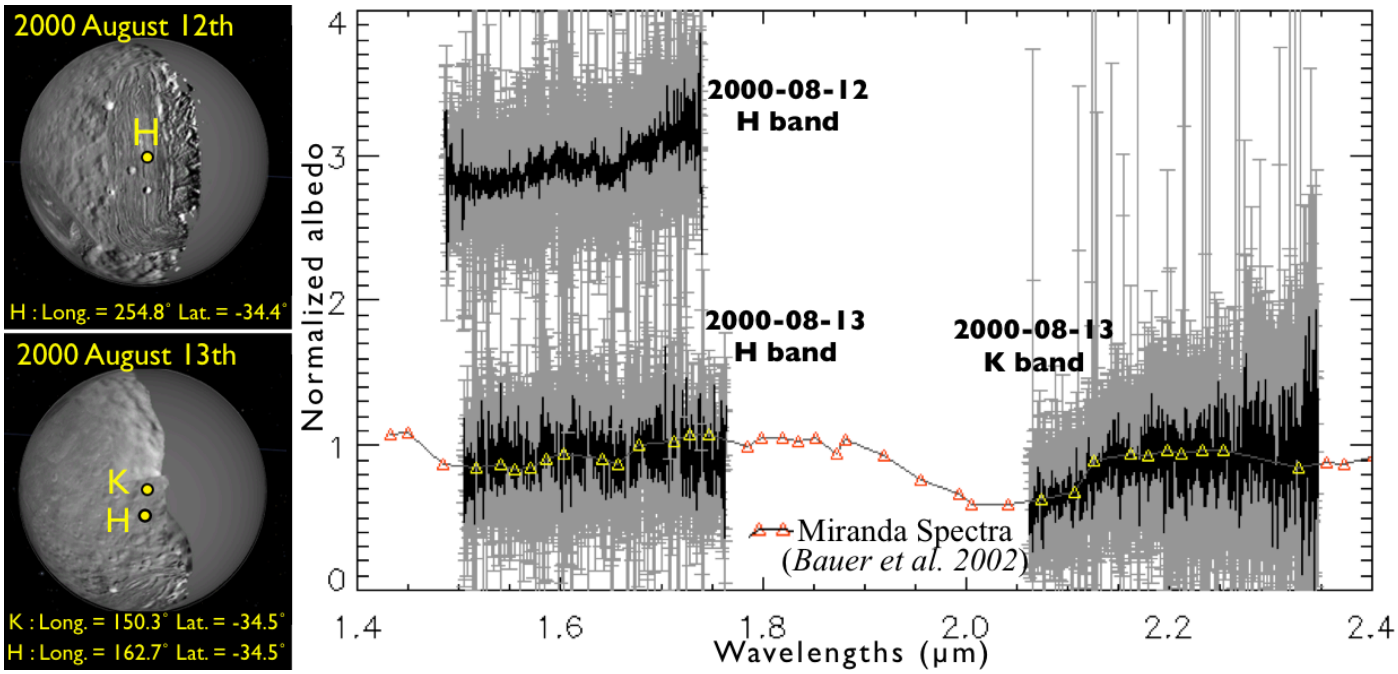


**Fig. 2.** *Left*: surface of Miranda[1] as observed from Palomar on the left side of the figure for both observing dates. The *H*-band spectrum of Miranda obtained on 2000 August 12 is shown at top, while the *H*- and *K*-band spectra collected on 2000 August 13 are shown at the bottom. The coordinates "Long." and "Lat." are respectively the apparent planetographic ("geodetic") longitude and the latitude (IAU2006 model) corresponding to the observations (yellow points) at both dates. The one-sigma error bars are also shown for our spectra (resolving power $\lambda/\Delta\lambda$ is about 1500). All spectra have been normalized to the data published by Bauer et al. (2002) (represented by the line curves with triangles). The top spectrum has been offset by +2.0 units along the *y*-axis for clarity. The regions with no data shown to correspond to high atmospheric opacity.

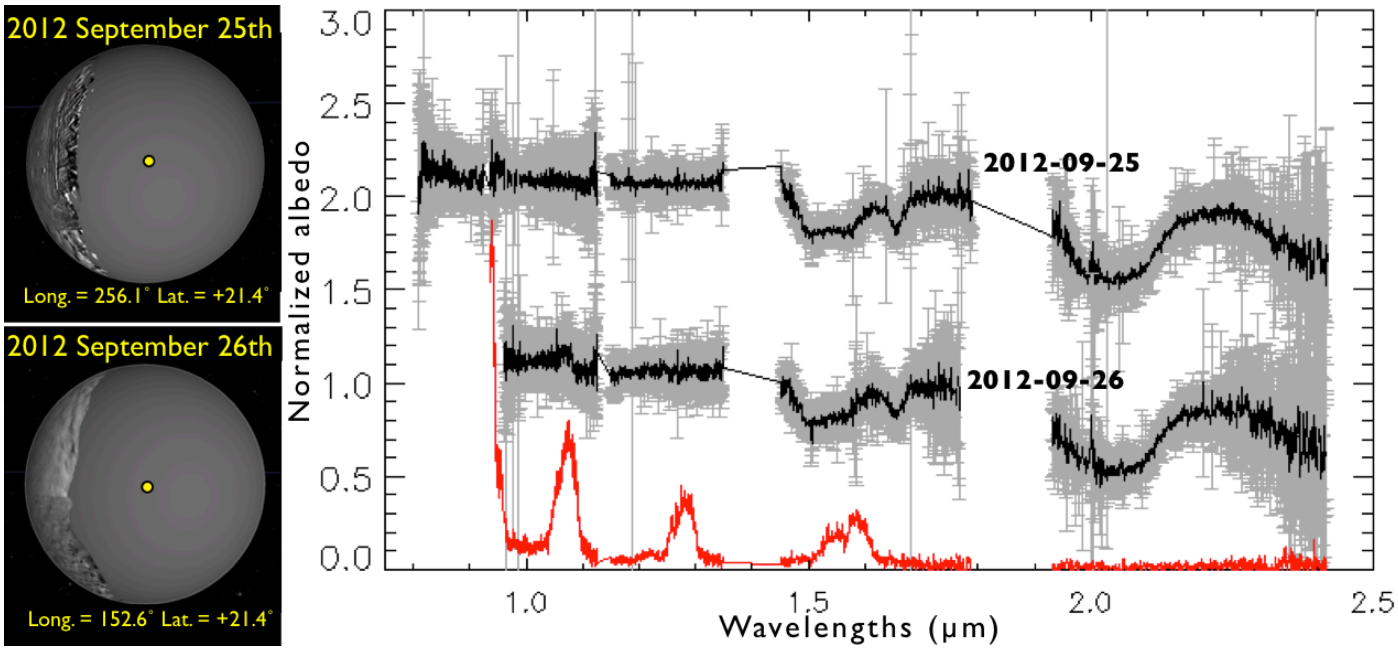


**Fig. 3.** *Left*: as for Fig. 2, but for the epochs of the IRTF observations. The 1-sigma error bar of our spectra is shown for both dates (resolving power $\lambda/\Delta\lambda$ is about 2000). The top spectrum has been offset by +1.0 units along the *y*-axis for clarity. The red curve on the bottom represents the location of the maximum of Uranus contamination (Sep. 26, 2012), which was subtracted from the spectrum.

of Miranda in comparison to the larger outer moons is likely to play a major role in facilitating the gravitational escape of $CO_2$ ice from its surface.

[1] The simulations were realized with NASA 3-D Environment: "Eyes on the Solar System" (http://solarsystem.nasa.gov/).

### *4.3. Modeling*

#### 4.3.1. Methods

We use the spectral model developed by Hapke (1981, 1993) to investigate the chemical properties of the compounds covering the surface of Miranda. This model allows us to constrain the reflectance spectra and the albedo of a medium using the physical

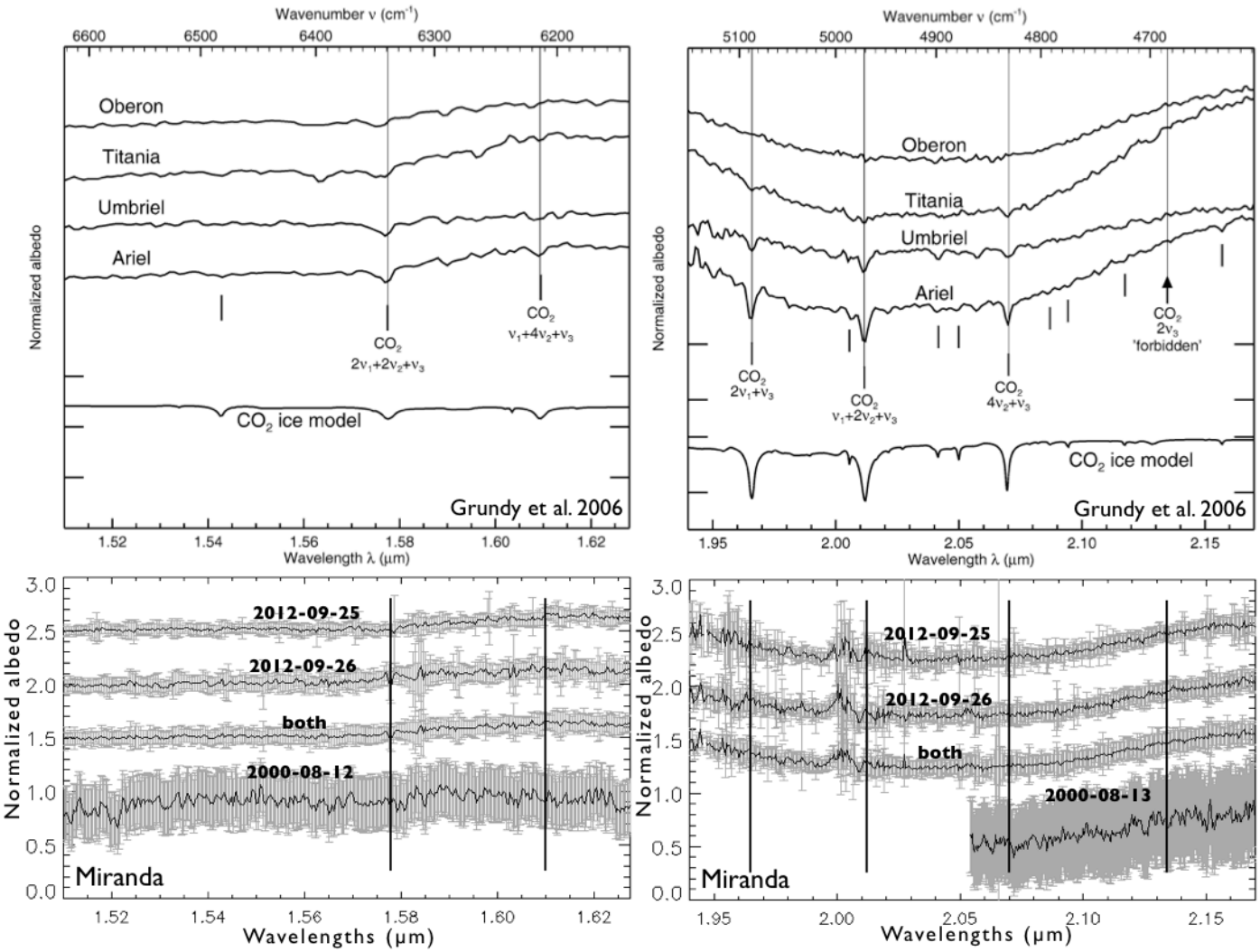


**Fig. 4.** *Top figure*: SpeX spectra of the three outermost moons of Uranus (Grundy et al. 2006) showing increasing abundance of $CO_2$ ice with decreasing planetocentric distances. *Bottom figure*: our PHARO and SpeX spectra (without the *H*-band spectra of 2000-08-13 due to some contamination by Uranus). The vertical solid lines represent the positions of the $CO_2$ bands (including a forbidden band).

properties of the different chemical components. The albedo is approximated using Eq. (44) of Hapke (1981),

$$Alb = r_0(0.5 + r_0/6) + (w/8)((1 + B_0)P(0) - 1), \quad (1)$$

where $w$ is the single-scattering albedo and $r_0$ the bihemispherical reflectance, which is purely single-scattering albedo-dependent:

$$r_0 = \frac{1 - \sqrt{1-w}}{1 + \sqrt{1-w}}, \quad (2)$$

where $w$ depends on the optical constants and the size of the particles and is computed for a multi-component surface (assumed to be intimately and/or geographically mixed, (see Poulet et al. 2002). Here, $B_0$ is the ratio of the near-surface contribution to the total particle scattering at zero phase angle and $P$ is the phase function. The method is described in Merlin et al. (2010), which uses an albedo-approximation model with a phase angle equal to 0, while $B_0$ is assumed to be close to 0.67 for icy objects (Verbiscer & Helfenstein 1998). The surface roughness and interference have been neglected in our work.

#### 4.3.2. Results for intimate mixtures

The free parameters are the asymmetry parameters of the phase function (which is approximated by a single Henyey-Greenstein function), the particle sizes and abundances. In addition to these initial free parameters, we also add two others ($a$ and $b$ thereafter) to adjust our model for the blue continuum of the spectrum with a two-degree polynomial curve (of the form $1 + ax + bx^2$). Here, $x$ is the wavelength given by $x = (\lambda(i) - 1.70)$ $\mu$m because we normalized the spectra at 1.70 $\mu$m with an albedo of 0.30. In each case, the model was applied to the IRTF spectra only (of higher S/N than the Palomar's spectra) as shown in Figs. 5a and b.

To determine the free parameters, we use a best fit model based on the Levenberg-Marquardt algorithm, which minimizes the reduced $\chi^2$. The minimization is applied outside the telluric absorption bands, which can affect the results. Best models are based on an intimate mixture of crystalline water ice (optical constants at 50 K from Grundy & Schmitt 1998), ammonia-hydrate (with only 1% of ammonia diluted in water, Brown et al. 1988), amorphous carbon (Zubko et al. 1996), and amorphous water ice (at low temperature, Mastrapa et al. 2008). The model applied to both spectra returns very similar results for the

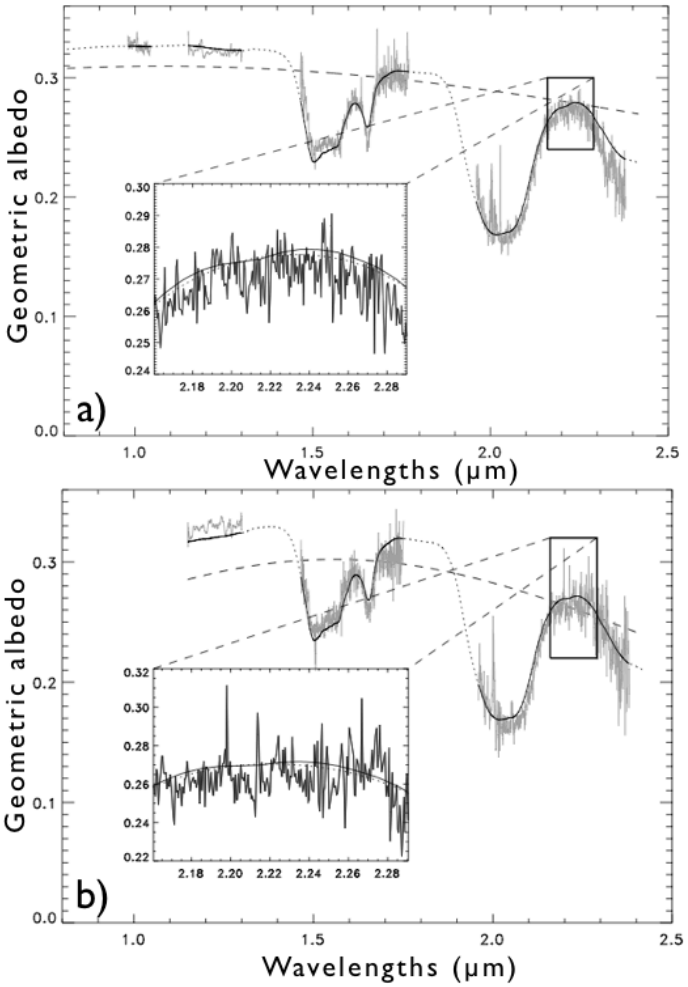


**Fig. 5.** **a)** Spectrum of Miranda taken on 2012 September 25 (trailing hemisphere) and the result of our spectral modeling. The fit is represented by continuous (fit to spectral data) and dotted lines (extrapolation to regions with no data). The dashed line represents the continuum, which has been fitted and implemented in the model to reproduce the blue slope in the near infrared. The window in insert covers the [2.16–2.30] $\mu$m range. Two models are presented, both made of water ice (crystalline and amorphous) and amorphous carbon. The solid line shows the ammonia hydrate included in the model, while the dotted line corresponds to the model without ammonia. Both models fit nearly equally our spectroscopic data. **b)** Similar representation as above, but for the spectrum obtained on 2012 September 26 (leading hemisphere).

compounds abundances, with almost 85% of crystalline water ice (4 $\mu$m grain size), 8% of ammonia hydrate (35 $\mu$m), 5% of amorphous carbon (10 $\mu$m), 2% of amorphous water ice (100 $\mu$m), and an asymmetry parameter comprised between 0.86 and 0.90. The main variation between the two is the values found for parameters used to fit the continuum. The coefficient $a = 0.1$ for both spectra, while $b = 0.08$ for the spectrum taken on September 25 (leading hemisphere) and $b = 0.35$ for the spectrum taken on September 26 (trailing hemisphere). Although we cannot ignore that this difference could be an artifact introduced by an incomplete background removal, we use the next section to discuss its possible origin, if real. Finally, we also studied the 2.22 $\mu$m region of the IRTF spectra in more detail, where the ammonia hydrate feature is expected to be present. For this we applied a second model (dotted line in the inserts of Fig. 5) based on the same mixture as described above, but with no ammonia hydrate. From these models, no hard conclusion can be derived about the presence of ammonia hydrate. Indeed, both models fit the data equivalently in the 2.22 $\mu$m region, the only difference being slightly improved reduced $Chi_2$ values (over the full spectral range) for both dates when ammonia is introduced into the model ($Chi_2 \sim 2.4$ with ammonia, and 2.7 (3.4) without ammonia for the IRTF spectra of 2012 September 25 (26) respectively). This result suggests that ammonia could be present on the surface of Miranda, but at low concentrations.

#### 4.3.3. Miranda's spectrum continuum

If the variation observed between the spectrum continuum of the leading and trailing hemispheres is real, it could be the result of spatial fluctuations in the abundance of "old" material and "fresher" internal ices across the surface. Indeed, Voyager 2 has shown that Miranda exhibits both old and young surface ices, with a series of features such as faults, craters, and large-scale upwelling, a remnant of a geologically very active past.

An alternative explanation could be the effect of weathering, induced by the impact of particles originating in the uranian magnetosphere, whose population is strongly affected by the Uranus moons that sweep through the magnetosphere, leaving noticeable gaps. The particle flux is high enough to cause darkening or space weathering of the moon's surfaces on a rapid timescale of 100 000 years (Krimigis et al. 1986). This phenomenon may be the cause of the dark coloration of the moons and rings, as well as of the observed leading-trailing compositional asymmetry seen on the outer moons. The magnetic field of Uranus rotates with the same period of 17.9 h as the planet, while the satellites orbit more slowly (orbital periods ranging from 1.41 to 13.46 days from Miranda to Oberon, respectively). As a result, the magnetospheric particles tend to bombard their trailing hemisphere (Cheng et al. 1986; Lanzerotti et al. 1987), which could explain the difference in slope continuum between our two spectra.

## 5. Conclusions

Spectroscopic data obtained with Palomar/PHARO and IRTF/SpeX show that a large part of Miranda's surface is covered by crystalline water ice. No significant spectral differences were observed between the young (coronae) and older regions, which exhibit the same icy components mixture dominated by a high (~85%) concentration of crystalline water ice. We also searched for volatiles in the spectrum of Miranda, and although we could not unambiguously detect the signature of ammonia hydrate, we cannot refute it. Similarly, we did not find any evidence of the presence of carbon dioxide ice. This result suggests that the presence of $CO_2$ on the surface of the Uranian satellites is not solely driven by their planetocentric distance. A full spectral mapping of the surface of Miranda is required to better diagnose of the chemical nature and physical states of the volatiles present on the surface of this intriguing satellite.

## References

Bauer, J. M., Roush, T. L., Geballe, T. R., et al. 2002, Icarus, 158, 178
Brown, R. H., & Clark, R. N. 1984, Icarus, 58, 288
Brown, R. H., & Cruikshank, D. P. 1983, Icarus, 55, 83
Brown, R. H., Cruikshank, D. P., Tokunaga, A. T., Smith, R. G., & Clark, R. N. 1988, Icarus, 74, 262
Buratti, B. J., & Mosher, J. A. 1991, Icarus, 90, 1

Cheng, A. F., Haff, P. K., Johnson, R. E., & Lanzerotti, L. J. 1986, in Satellites, eds. J. A. Burns, & M. S. Matthews (Tucson: Univ. Arizona Press), 403
Crida, A., & Charnoz, S. 2012, Science, 338, 1196
Cushing, M. C., Vacca, W. D., & Rayner, J. T. 2004, PASP, 116, 362
Grundy, W. M., & Schmitt, B. 1998, J. Geophys. Res., 103, 25809
Grundy, W. M., Young, L. A., Spencer, J. R., et al. 2006, Icarus, 184, 543
Hapke, B. 1993, Theory of reflectance and emittance spectroscopy, ed. B. Hapke (Cambridge: Cambridge University Press)
Jacobson, R. A., Campbell, J. K., Taylor, A. H., & Synnott, S. P. 1992, AJ, 103, 2068
Karkoschka, E. 1997, Icarus, 125, 348
Krimigis, S. M., Armstrong, T. P., Axford, W. I., Cheng, A. F., & Gloeckler, G. 1986, Science, 233, 97
Lanzerotti, L. J., Brown, W. L., Maclennan, C. G., Cheng, A. F., & Krimigis, S. M. 1987, J. Geophys. Res., 92, 14949
Mastrapa, R. M., Bernstein, M. P., Sandford, S. A., et al. 2008, Icarus, 197, 307
Merlin, F., Barucci, M. A., de Bergh, C., et al. 2010, Icarus, 208, 945
Metchev, S. A., & Hillenbrand, L. A. 2004, ApJ, 617, 1330
Poulet, F., Cuzzi, J. N., Cruikshank, D. P., Roush, T., & Dalle Ore, C. M. 2002, Icarus, 160, 313
Rayner, J. T., Toomey, D. W., Onaka, P. M., et al. 2003, PASP, 115, 362
Seidelmann, P. K., Archinal, B. A., A'Hearn, M. F., et al. 2007, Celest. Mech. Dyn. Astron., 98, 155
Tittemore, W. C., & Wisdom, J. 1990, Icarus, 85, 394
Trilling, D. E., & Brown, R. H. 2000, Icarus, 148, 301
Verbiscer, A., & Helfenstein, P. 1998, in Solar System Ices, eds. B. Schmitt, C. de Bergh, & M. Festou, Astrophys. Space Sci. Lib., 227, 157
Zubko, V. G., Mennella, V., Colangeli, L., & Bussoletti, E. 1996, MNRAS, 282, 1321